



2nd Advanced Optical Metrology Compendium

Advanced Optical Metrology

Geoscience | Corrosion | Particles | Additive Manufacturing: Metallurgy, Cut Analysis & Porosity



EVIDENT
OLYMPUS

WILEY

The latest eBook from **Advanced Optical Metrology**.
Download for free.

This compendium includes a collection of optical metrology papers, a repository of teaching materials, and instructions on how to publish scientific achievements.

With the aim of improving communication between fundamental research and industrial applications in the field of optical metrology we have collected and organized existing information and made it more accessible and useful for researchers and practitioners.

EVIDENT
OLYMPUS

WILEY

Achieving Low-Voltage Operation of Intrinsically-Stretchable Organic Light-Emitting Diodes

Shin Jung Han, Huanyu Zhou, Hyeokjun Kwon, Seung-Je Woo, and Tae-Woo Lee*

A minimum operating voltage of intrinsically-stretchable organic light-emitting diodes (ISOLEDs) is always required for practical applications. However, the lack of protocols for the lamination complicates the task of attaining a reliable ISOLED without inducing degradation. Here, a solvent-vapor-assisted lamination (SVL) method to reinforce the cathode interface is presented; this process lowers the operation voltage and increases the stretchability of ISOLEDs. Achieving a uniform contact and strong adhesion at the interface is the key to attaining reliable lamination. A cold-pressing (CP) treatment is applied first to reduce the surface roughness of silver nanowires before the surface embedding process. A subsequent solvent vapor treatment before the lamination partially solvated the surface of the active layer with an increase in the segmental motion of polymer chains, which substantially increases the interfacial adhesion after lamination. The combination of CP and SVL treatments considerably reduces threshold voltage V_{th} (i.e., voltage at which current shows an abrupt increase for light-emission) from 6.7 to 2.7 V. The ISOLED also exhibits excellent mechanical stretchability, with no significant change in luminance under 30% strain. This study can assist in the development of practical applications of intrinsically-stretchable optoelectronic devices.

1. Introduction

Wearable electronics systems integrated with on-skin sensors and stretchable displays can be used to continuously monitor and visualize physiological signals.^[1–15] However, despite the significant improvement in the stretchability of electronic devices, the development of intrinsically-stretchable displays has stagnated because they have high operating voltages that are not suitable for wearable applications.^[16–21] The state-of-the-art stretchable displays that consist of fully-stretchable layers can be easily stretched > 100%, but are normally oper-

ated under an AC electric field of several kilovolts by using a high-voltage amplifier. As an alternative, DC-driven ISOLEDs are preferred, because they can be operated at low voltages, so they are more promising candidates for practical applications. Nonetheless, few papers have reported on ISOLEDs that use intrinsically-stretchable light-emitting layers and electrodes since 2011.^[22–29] The reported DC-driven ISOLEDs still suffer from the high $V_{on} > 5$ V that strongly depends on the quality of the contact between the stretchable cathode and light-emitting materials.


Direct coating of conductive nanomaterial composites can be used to form an electrical contact at the interface, but this method requires a careful selection of the solvent for electrode deposition.^[26] Alternatively, a free-standing stretchable cathode can be prepared on another substrate and then contacted onto the active layer with heat T and pressure P to enhance the adhesion strength.^[28]

However, the rough surface of the stretchable electrode at the laminated interface and its huge difference in surface energy from the underlying organic layer causes poor adhesion, which requires fine-tuning of the lamination conditions. Due to difficulties in quantifying the lamination quality, excess T , P , or both are often applied during lamination to improve stretchability, but these treatments induce a significant decrease in conductivity of electrodes and photoluminance (PL) intensity of the light-emitting layer.^[28,30,31] Therefore, the excess T and P substantially increase the V_{on} and decrease the device efficiency. Simultaneous attainment of low V_{on} and excellent stretchability with a firmly laminated interface remains a challenge; overcoming it requires development of new methods to eliminate those demerits.

Here, we present a solvent-vapor-assisted lamination (SVL) method to reinforce the weakly laminated stretchable cathode interface. This method substantially increases the mechanical stretchability and lowers the operation voltage of the ISOLEDs. Achieving a uniform contact and strong adhesion at the interface is the key to attaining reliable lamination. A cold-pressing (CP) treatment was introduced to reduce the surface roughness R_{rms} of silver nanowires (AgNWs) before the embedding process, which enables the stretchable cathode to form a uniform contact at the laminated interface. After the subsequent SVL treatment, an increase in adhesion of the laminated interface is attributed to the increase in segmental motion of polymer

S. J. Han, H. Zhou, H. Kwon, S.-J. Woo, T.-W. Lee
Department of Materials Science and Engineering
Seoul National University
Seoul 08826, Republic of Korea
E-mail: twlees@snu.ac.kr

T.-W. Lee
School of Chemical and Biological Engineering
Institute of Engineering Research
Research Institute of Advanced Materials
Soft Foundry
Seoul National University
Seoul 08826, Republic of Korea

 The ORCID identification number(s) for the author(s) of this article can be found under <https://doi.org/10.1002/adfm.202211150>.

DOI: 10.1002/adfm.202211150

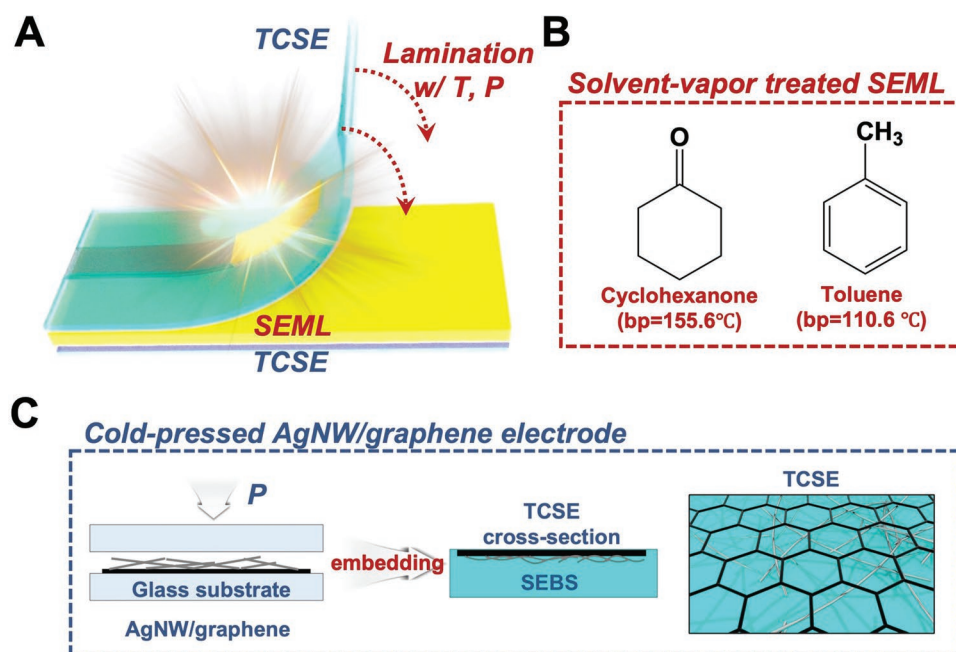


Figure 1. A) Schematic illustration of cathode lamination process with the application of heat T and pressure P to obtain a firmly-laminated interface. 2D contact stretchable electrodes (TCSEs) as the anode and the cathode. B) Chemical structures and boiling point (bp) of solvents used for vapor treatment before the lamination process. C) Conceptual illustration of a cold-pressing method to reduce the surface roughness of AgNW/graphene electrode before surface embedding.

chains in the partially-solvated active layer. A cross-hatch pattern analysis method is also proposed to quantify the adhesion properties of the laminated interface. The combination of CP and subsequent SVAL treatments substantially decrease the threshold voltage V_{th} from 6.7 to 2.7 V. The ISOLED also exhibits excellent mechanical stretchability, with no significant change in luminance under 30% strain.

2. Results and Discussion

AgNW percolation networks are normally embedded in the elastomer near-surface region to attain stretchability. Nonetheless, the electrical conduction within the stretchable electrode can occur only along the wire, and the contact area between half-buried AgNW networks and the adjacent organic material is limited.^[28] Hence, charge spreading in a lateral direction within stretchable electrodes using AgNWs and charge injection in a vertical direction from the stretchable electrodes have been inefficient in OLEDs. To boost the electroluminescence efficiency of the ISOLED, we previously developed a 2D contact stretchable electrode (TCSE) as both anode and cathode.^[28] Graphene was introduced on the surface of embedded AgNW networks to form a 2D contact with the organic material. The graphene interlayer significantly increased charge spreading for better conduction, work function tunability, and contact area of the TCSE, resulting in an improvement in the device's current efficiency.^[28]

To fabricate an ISOLED, the cathode TCSE was formed on another substrate, and adhered to the stretchable light-emitting layer (SEML) by applying T and P ; this process is known

as cathode lamination (Figure 1A). Adhesion at the interface between TCSE and SEML requires both strong interactions across the interface and a uniform contact area. Whereas, applying excess T , P , or both during lamination to increase interfacial adhesion can deteriorate the conductivity of the electrode and the light-emitting property of SEML and thereby degrade the device's electrical characteristics. SVAL was, therefore, developed to reinforce a weakly-laminated interface to attain improved stretchability without inducing any degradation during lamination. Light-emitting polymers are mostly dissolved in non-polar solvents, so toluene and cyclohexanone, which have different boiling points (bps) were chosen as solvents for the solvent vapor treatment (Figure 1B). The segmental motion of polymer chains from the partially-solvated SEML surface is increased, so the polymer chain entanglement and interfacial adhesion also increase.

Forming a uniform contact at the laminated interface is vital for attaining strong interfacial adhesion. The CP process was used to reduce R_{rms} of randomly-distributed AgNW percolation networks and thereby improve lamination quality (Figure 1C). AgNWs commonly suffer from high junction resistance,^[32] so post-fabrication thermal annealing on AgNWs was used to weld the AgNW/AgNW junctions and reduce R_s . Thermal annealing has a more dominant effect than CP treatment on R_s , so the effects of thermal annealing and CP on R_s of AgNW/graphene electrodes were evaluated separately.

R_s of the AgNW/graphene electrode substantially reduced from $38.4 \Omega \text{ sq}^{-1}$ at 25°C to $21.4 \Omega \text{ sq}^{-1}$ after thermal annealing at 150°C for 5 min (Figure 2A); this change indicates a reduction in contact resistance at the welded AgNW junctions. With further increasing annealing temperature to 200°C , AgNWs

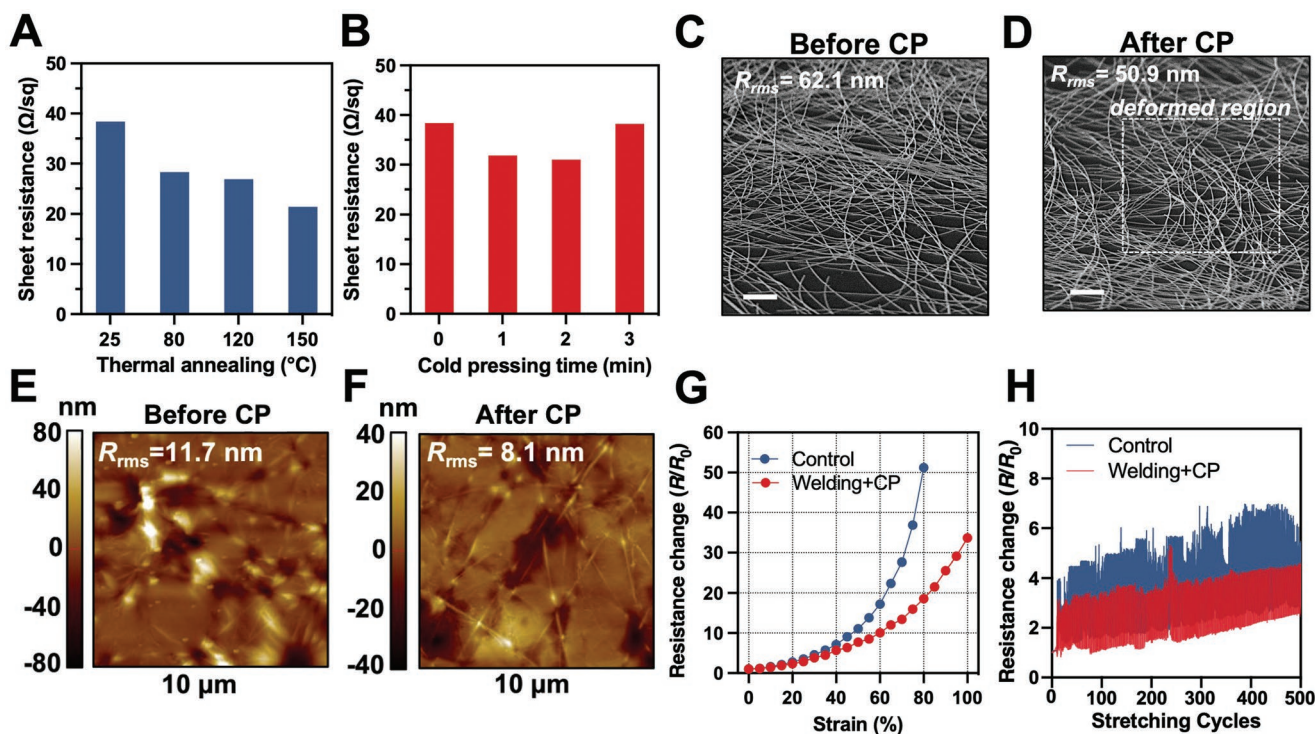


Figure 2. Evolution of sheet resistance of AgNW/graphene electrode on a glass substrate in terms of A) thermal annealing at the desired temperature for 5 min, and B) increasing CP time at 50 kPa pressure without thermal annealing. C, D) SEM images of AgNW/graphene electrodes before and after CP. Scale bar: 1 μm . Dashed square encloses AgNWs that had been deformed by CP. E, F) AFM topography images (scan size: $10 \times 10 \mu\text{m}$) of AgNW/graphene electrode before and after CP. G) Static stretching and H) cyclic stretching tests (tensile strain = 40%) of the TCSE without any treatments (control) and the one with both thermal welding and CP treatments.

melted and became disconnected in the OM image (Figure S1, Supporting Information); this change led to increased R_s by a few orders of magnitude. Welding of AgNWs before embedding into the elastomer can prevent AgNWs from disconnecting and sliding at the junction, and thereby increases stretchability.^[25] Then the effect of CP was evaluated using pristine AgNW/graphene without thermal annealing as the reference. R_s of the AgNW/graphene electrode declined by 19.1% after 2 min of CP at 50 kPa (Figure 2B) but increased to $38.2 \Omega \text{sq}^{-1}$ after CP for 3 min. The change in morphology of AgNW/graphene before and after CP indicates that the deformation of AgNWs by pressure increased the compactness of structure with the underlying graphene layer (Figure 2C,D). The protrusions of the AgNW networks can be effectively removed after applying mechanical compressive stress, as confirmed by the deformation of AgNWs. The CP treatment significantly decreased R_{rms} of the AgNW/graphene electrode from 62.1 to 50.9 nm. However, severe deformation of AgNWs after 3 min of CP could degrade the electrical conduction along a wire; this change causes an increase in R_s . For these reasons, we chose 2 min for the CP process. After embedding AgNW/graphene in styrene-ethylene-butadiene-styrene (SEBS) elastomer matrix, the R_{rms} of TCSE after CP substantially decreased from 11.7 to 8.1 nm in a $10 \times 10 \mu\text{m}$ scan (Figure 2E,F). Hence, the optimal post-fabrication treatment on AgNW/graphene was identified as thermal annealing at 150 $^{\circ}\text{C}$ for 5 min, followed by 2 min of CP at 50 kPa; this process caused a slight decrease in R_s to $21.0 \Omega \text{sq}^{-1}$.

The mechanical stretchability of the TCSE with and without any post-treatments was evaluated. At 20% static strain, the normalized resistance change (R/R_0) of TCSE with thermal welding and CP treatments only increased by 132%, whereas the control electrode showed a 181% increase (Figure 2G). The same trend was also observed in the cyclic stretching test at 40% strain (Figure 2H), proving that the combination of thermal welding and CP treatments substantially suppressed the sliding of the AgNWs and increased the stretchability of the TCSE.

Then the effects of temperature and duration of lamination were evaluated by measuring the contact resistance R_c of two TCSE that faced each other. Lamination temperature was decided considering the glass transition temperatures T_g of components in the SEML. The segmental motion of the polymer chain increases at $T > T_g$, and this motion increases interchain diffusion with a firmly laminated interface. Polyethylene oxide (PEO) and polyethyleneimine (PEI) which were used in this work both have $T_g < 0 \text{ }^{\circ}\text{C}$, so the chain mobility was assumed to be high at room temperature. However, the light-emitting polymer (Super Yellow) has the highest $T_g = 85 \text{ }^{\circ}\text{C}$, the lamination temperature should be maintained $> 85 \text{ }^{\circ}\text{C}$ to ensure high polymer chain segmental motion but without inducing degradation in the electrical conductivity of TCSEs. Conductive surfaces of TCSEs were placed facing each other, and R_c was measured while T was increased from 90 to 130 $^{\circ}\text{C}$. The lowest R_c was attained after one-time lamination at 100 $^{\circ}\text{C}$; this result indicates that the TCSE forms a good electrical

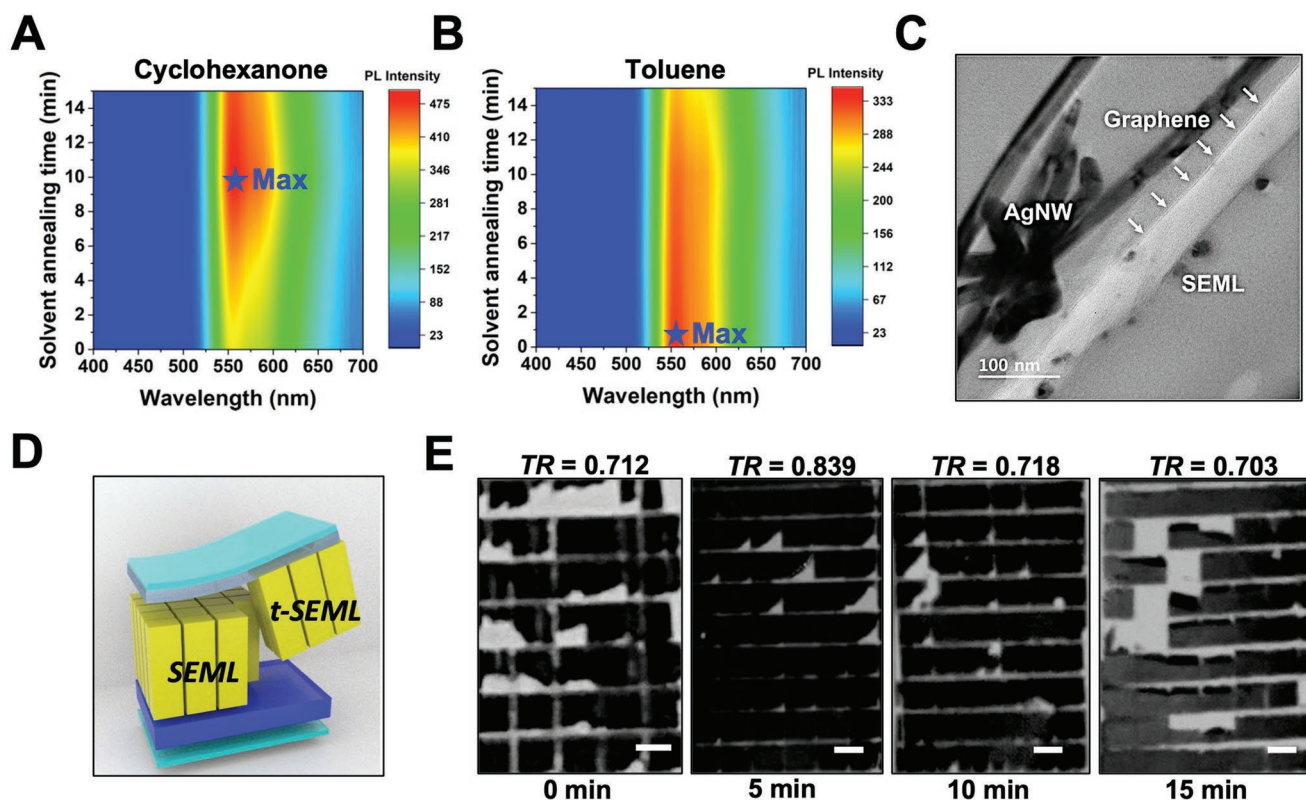


Figure 3. Photoluminance (PL) color plot after applying increasing duration of solvent vapor treatment using A) cyclohexanone, and B) toluene. C) transmission electron microscopy cross-section images of the interfaces in the IsoleDs. D) Schematic illustration of the cross-hatch adhesion test. *t*-SEML stands for stretchable SEML transferred to the TCSE after the adhesion test. E) Image analysis on the releasing substrate after detaching the cathode TCSE with increasing cyclohexanone solvent treatment time. Scale bar: 1 μ m.

contact without any degradation at the interface (Figure S2A, B, Supporting Information).

Except for a uniform and flat stretchable electrode surface, increasing the interchain diffusion of polymer chains is also important to obtain a firmly laminated interface. Maintaining lamination temperature $> T_g$ increases the mobility of the polymer chain, whereas a firmly-laminated interface without inducing degradation in device V_{on} cannot easily be obtained. Hence, monitoring variations of the photoluminance (PL) spectrum may be an indirect way to quantify the lamination quality. Toluene (bp = 110.6 $^{\circ}$ C) and cyclohexanone (bp = 155.6 $^{\circ}$ C) were chosen as solvents because they are commonly used to dissolve Super Yellow. To perform the solvent-vapor treatment, solvents were pre-heated separately in closed Petri dishes at 100 $^{\circ}$ C for > 5 min, then TCSE coated with the SEML was heated to form a partially-solvated surface. The difference in bps of the solvents caused opposing trends in PL of the SEML during the solvent vapor treatment. The use of cyclohexanone yielded a constant increase in PL intensity (Figure 3A) whereas the use of toluene yielded a decrease (Figure 3B). Normalized PL spectra of the same processes showed the same result (Figure S3, Supporting Information).

The presence of solvent on the SEML protects it from contact with air and thereby avoids exciton quenching induced by oxygen. Solvent annealing using cyclohexanone for 5 min was the optimal condition for the lamination.^[33] However, due to the low bp of toluene, it readily evaporates when heated at 100 $^{\circ}$ C, and does not solvate the SEML surface. Cross-sections of lami-

nated IsoleDs were analyzed to confirm the quality of the interface after lamination. The specimen was prepared using a focused ion beam, then analyzed using high-resolution transmission electron microscopy (HR-TEM) (Figure 3C). The TEM images showed no voids at the interface; this absence indicates that the TCSE formed intimate contact with the SEML layer.

To quantify the interfacial adhesion strength using the adhesion test, we developed a cross-hatch pattern-transfer method (Figure 3D). The pattern created on the SMEL was intended to exclude the effect of the cohesion force of the SEML during the adhesion test (Figure S4, Supporting Information). The area of the transferred SEML (*t*-SEML, dark area) was measured using image analysis after the monochrome adjustment to obtain a high image contrast. The strength of the adhesion was quantified using the transfer rate *TR*, which was defined as the ratio of the area of transferred SEML (*t*-SEML) to the total area of SEML. A high *TR* means a strong adhesion at the laminated interface. The SVAL treatment using cyclohexanone for 5 min gave the highest *TR* = 0.839 (Figure 3E), while the SVAL treatment using toluene for 5 min gave significantly lower *TR* = 0.543 (Figure S5, Supporting Information). The difference in *TR* indicates that the laminated interface after SVAL using toluene was weak, and this inference is consistent with the PL contour plots of solvent annealing using different solvents (Figure 3A,B). Therefore, the adhesion test reveals that the SVAL using cyclohexanone gives the best adhesion strength at the laminated interface, which is beneficial for the IsoleD operation.

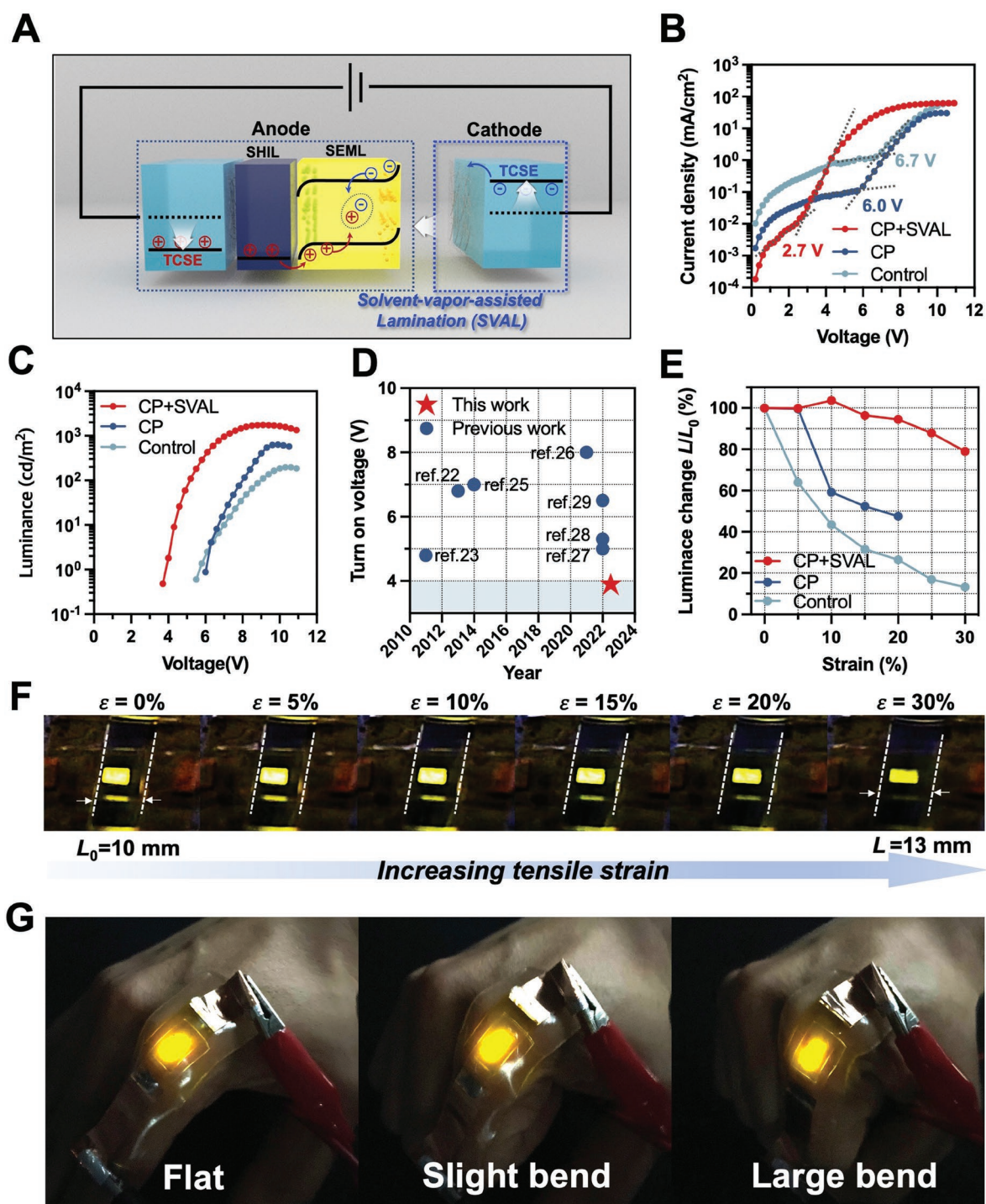


Figure 4. A) Schematic image of ISOLED architecture fabricated using SVAL. SHIL: stretchable hole injection layer; SEML: stretchable light-emitting layer (see Experimental Section for more details). B) Current density–voltage (J – V), and C) luminance–voltage (L – V) of control ISOLED without any treatment, the ISOLED with CP and the ISOLED with both CP and SVAL. D) Progress in the development of turn-on voltage V_{on} of ISOLEDs. E) Change in luminance of the control ISOLED, the one with only CP, and the one with both CP and SVAL treatments at 6 V under uniaxial tensile strain. F) Digital images of the ISOLED with both CP and SVAL treatments under tensile strain from 0 to 30% at 6 V. G) Digital images of the ISOLED with both CP and SVAL treatments on a joint withstanding various deformations when the user makes a fist.

When the voltage is applied to the ISOLED, ions in the SEML dissociate and drift to the opposite electrode to form electric double layers (EDLs) that can induce severe band bending at

electrode interfaces (Figure 4A). This response facilitates charge injection without the need for a sophisticated device structure.^[34] Current density–voltage (J – V) relationships, especially

at low operation voltage before turn-on, imply that the interface formed after CP and SVAL treatments is highly uniform with low leakage current when compared with the control group without any additional treatment (Figure 4B). In the J - V curve with both CP and SVAL treatments, two sudden increases in J , one between 0 and 1 V and one at > 2.7 V, are consequences of charge injection of holes and electrons, respectively. In Super Yellow, holes are more mobile than electrons,^[35] so the rate of charge injection is limited by electron transport. But the V_{th} of the control ISOLED, and the one with only CP are as high as 6.7 and 6.0 V, respectively, which implies that both CP and SVAL treatments can significantly reduce the V_{th} with a better electron injection capability. The luminance-voltage (L - V) also exhibited the same trends as the J - V characteristics. The emitted light was detected using the spectroradiometer at $V_{on} = 3.7$ V with the maximum luminance $L_{max} = 1754$ cd m⁻² after SVAL (Figure 4C). To our best knowledge, this is the lowest V_{on} among all reported ISOLEDs (Figure 4D; Table S1, Supporting Information). Currently, the device efficiency, L_{max} , and even the lifetime of ISOLEDs are far lower than those of the state-of-the-art ITO-based phosphorescent OLEDs which have a maximum luminance of over 10 000 cd m⁻². However, the record luminance value in the ISOLEDs up to now is only 7450 cd m⁻².^[27] We have summarized the characteristics of most reported ISOLEDs and added them to the supporting information (Table S1, Supporting Information).

The charge injection property of the electrodes in the ISOLED was compared with an ITO electrode that has the same device architecture except for the cathode. The ITO-based device had a lower V_{th} of 2.0 V than that of the ISOLED (Figure S6, Supporting Information); the difference is mainly induced by the difference in the electron injection barriers. The LiF/Al is a well-known cathode material that can significantly reduce the height of the electron injection barrier,^[36] whereas the AgNW/graphene (called TCSE in this work) with only PEI as the interlayer showed a work function of 4.04 eV,^[28] which makes electron injection in the ISOLED a recombination rate-determining step for light-emission. Also, the voltage at which a current efficiency is a maximum was lower in the ITO device than in the ISOLED, proving that the LiF/Al electrode has better electron injection property than the TCSE. Given the situation, the low V_{th} of the ISOLED (2.7 V) is achieved, which is slightly higher than that of the ITO device (2.0 V). Comparison of the J - V - L characteristics of the ISOLED with those of the ITO-based device demonstrates that the suggested SVAL treatment yields a laminated cathode that functions well.

Before the ISOLED stretching test, microstructures of the stretchable organic layers were analyzed. The inclusion of non-ionic surfactant Triton-X into poly(3,4-ethylenedioxythiophene);polystyrene sulfonate (PEDOT:PSS) facilitates the self-assembly of PEDOT and PSS chains to yield a stretchable hole injection layer (SHIL, Figure S7A,B, Supporting Information). The SEML that is deposited on the SHIL is incorporated with polyethylene oxide (PEO) and salts to form a stretchable solid-state electrolyte. The stretchability of SEML originates from an interpenetrating polymer network in which Super Yellow forms a continuous network and the soft ionic conductive phase PEO fills the pores, in a way that mimics a sponge immersed in water.^[37] As a result of the huge difference in polarities of Super

Yellow and PEO, strong phase separation was induced between the Super Yellow and the soft ionic phase that contains PEO and KCF₃SO₃ (Figure S7C,D, Supporting Information). Benefit from the microstructural engineering on SHIL and SEML, an in-situ tensile stretching test of the SHIL/SEML/PEI film on a homemade stretcher measured a crack-onset strain of $\approx 70\%$ (Figure S8, Supporting Information).

The ISOLEDs were sandwiched between two layers of 3 M VHB tape to protect them from exposure to air before the stretching test. The initial luminance (100%) of the ISOLED showed a slight decrease only to 94% after the application of 20% strain, and the light-emission spectrum did not change (Figure 4E). With a further increase in strain to 30%, the ISOLED treated with CP and SVAL showed negligible degradation (Figure 4F). However, the control ISOLED and the one with only CP degraded rapidly as the strain was increased up to 20%. This difference in stretchability is attributed to the interface reinforced by the SVAL.

Attaining highly reliable ISOLEDs under cyclic stretching test is still a challenging task. The best reported cyclic stretchability of ISOLED using the lamination method showed a 43% decrease in luminance after only 50 stretching and releasing cycles at 10% of strain in the nitrogen-filled glove box.^[22] Despite excellent static stretchability of the ISOLED after both CP and SVAL treatments (Figure 4E), the L of ISOLED decreased to 73% after 10 cycles of stretching at 20% of strain; compared with the normalized luminance change of the ISOLED under a constant voltage at 8 V in air, this might be caused by both poor reliability of the 3 M VHB tape encapsulation and mechanical degradation in the device during stretching test in air (Figure S9, Supporting Information). 3 M VHB tape is a poor barrier to oxygen and moisture, so the L of ISOLED at 8 V showed a monotonic decline after reaching the maximum luminance L_{max} and degraded to 50% within 2 min (Figure S9, Supporting Information). The effect of cyclic mechanical strain cannot be easily distinguished from degradation caused by air. However, to demonstrate the stretchability of the ISOLED, it has been placed onto the joint of hand, allowing it to withstand large deformation when the hand makes a fist (Figure 4G).

Appropriate encapsulation can effectively delocalize the strain around minor defects and suppress crack formation in the film.^[38] Hence, stretchable encapsulation design is critical to the cyclic stretchability of the device. Stretchability requires the encapsulant to be as amorphous as possible, but this requirement conflicts with the need for a highly-crystalline polymer structure to provide a good barrier to oxygen and water. These two properties are always in conflict, and to meet both simultaneously requires innovations in encapsulation material design.

3. Conclusion

We present an SVAL method to reinforce a weakly laminated cathode interface, thereby substantially increasing the mechanical stretchability, and lowering the V_{on} of ISOLEDs. Achieving a uniform contact and strong adhesion at the interface is the key to attaining reliable lamination. The CP treatment has

significantly reduced R_{rms} , so the stretchable cathode can form uniform contact with the laminated interface. After subsequent SVAL using cyclohexanone with a high boiling point, the surface of the SEML was partially solvated and the segmental motion of polymer chains was increased; these changes substantially reinforce the weakly laminated interfaces. The cross-hatch pattern analysis we propose here well quantified the adhesion properties of the laminated interfaces after SVAL. The CP and subsequent SVAL substantially decrease the V_{th} from 6.7 to 2.7 V. The ISOLED showed no significant change in luminance under 30% strain, i.e., has excellent mechanical stretchability. This work will provide a solution to the chronic adhesion problem that occurred at the laminated stretchable cathode interface of ISOLEDs, and will stimulate academic and industrial research on the fundamentals of stretchable optoelectronics for practical applications.

4. Experimental Section

Graphene synthesis and transfer process were described previously.^[28] Pristine AgNW solution (30 nm in diameter, 30 μ m in length, Novaral, 5 mg mL⁻¹ dispersed in isopropyl alcohol) was diluted to 2.5 mg mL⁻¹ to increase the uniformity of the AgNW electrode. The diluted AgNW solution was spin-coated on top of graphene at 2000 rpm for 60 s twice, then the combination was heated at 150 °C for 5 min to evaporate the residual solvent and weld the junctions between AgNWs. To reduce sheet resistance R_s of the TCSE, a portable hot-press machine was used for the CP process. The surface of AgNW/graphene was covered with another glass substrate, which was then pressed at 50 kPa for 2 min to flatten the surface of AgNW percolation networks and reduce R_s . Then styrene-ethylene-butadiene-styrene (SEBS, 180 mg mL⁻¹ in toluene) was drop-cast on the as-prepared AgNW/graphene substrate and left in ambient air to allow the solvent to evaporate. Then the substrate was released from the glass substrate in water with AgNW and graphene fully embedded in SEBS.

To prepare a stretchable hole injection layer (SHIL), 5 wt% of Triton X-100 was added to a 1:1 weight ratio solution of poly(3,4-ethylenedioxythiophene):poly(styrenesulfonate) (PEDOT:PSS, Clevios P VP AI4083) in isopropyl alcohol. The stretchable light-emitting layer (SEML) solution was a blend of Super Yellow (Merck, PDY-132, 10 mg mL⁻¹ in cyclohexanone), polyethylene oxide (PEO, MW = 5m, 10 mg mL⁻¹ in cyclohexanone), and potassium trifluoromethanesulfonate (KCF₃SO₃, 10 mg mL⁻¹ in cyclohexanone) at a volume ratio of 10:6:1. Perfluorinated sulfonic acid (PFSA, 2 wt% in IPA) and polyethyleneimine (PEI, Sigma, 3 wt% in 2-methoxyethanol) solutions were prepared as the *p*- and *n*-type dopant respectively for the TCSEs.

The TCSE with PFSA coating was used as the anode, and the TCSE with PEI coating was used as the cathode. The SHIL was spin-coated onto the TCSE anode at 1000 rpm for 60 s and then annealed at 90 °C for 5 min in ambient air. A successive coating of SEML at 3000 rpm for 60 s was performed under an N₂ atmosphere in a glove box with both O₂ and H₂O < 1 ppm. The resultant thickness of SEML was \approx 200 nm. Then the substrate was kept in a closed Petri dish on a hot plate at 100 °C with an open plastic Petri dish (60 \times 15 mm) filled with desired organic solvents for 5 min. The organic solvent partially solvated the surface of the SEML, thereby increased the adhesion at the interface. The treated specimen was taken out swiftly, then pre-contacted with the active layer by application of gentle pressure in the glove box. The specimen was hot pressed at 50 kPa and 100 °C for 5 min in ambient air by using the hot-press machine, then encapsulated using 3 M VHB tape. The reference structure fabricated on ITO substrate was the same as that of ISOLED except for the cathode. After coating of SEML, LiF (1 nm) and Al (100 nm) were sequentially deposited using a thermal evaporator.

The surface topographic images of TCSEs before and after CP were obtained by atomic force microscopy (NX-10, Park Systems). Surface morphologies of TCSE before and after CP were compared using scanning electron microscopy (SEM). Optical microscopy was also used to characterize the change in AgNW before and after thermal annealing. The R_{rms} of materials for the ISOLED were characterized using atomic force microscopy (NX-10, Park Systems). A cross-section sample of ISOLED was prepared using a focused ion beam (FIB, SMI3050E), then analyzed using TEM (JEM-2100F) with a beam energy of 30 kV. For static stretching test, tensile strain was applied to the electrode using a homemade stretcher at 20 mm min⁻¹. The cyclic stretching test on the electrode was conducted from 0 to 40% for 500 cycles at 100 mm min⁻¹. The change in resistance was measured using a digital multimeter (Keithley 6500) in real time.

The *J*-*V*-*L* characteristics of ISOLED were measured using a spectroradiometer (CS2000, Konica Minolta) combined with a source meter. For the stretching test, the strain was applied using a homemade stretcher with a Maya 2000 spectrometer placed right on the top of the ISOLED. The whole stretching system was placed in a dark box to exclude the effect of light from the environment.

To evaluate the adhesion at the interface between SEML and TCSE, a cross-hatch pattern was created using stacked razor blades with a 1-mm separation. The pattern was created to exclude the effect of cohesion forces within the film. After the SVAL process, the TCSE was peeled off slowly.

Supporting Information

Supporting Information is available from the Wiley Online Library or from the author.

Acknowledgements

S.J.H. and H.Z. contributed equally to this work. This work was supported by National Research Foundation of Korea (NRF) grant funded by the Korea government (Ministry of Science, ICT & Future Planning) (2016R1A3B1908431), LG Display under LGD-SNU Incubation Program (2021005682), Creative Materials Discovery Program through the National Research Foundation of Korea (NRF) funded by Ministry of Science and ICT (2018M3D1A1058536). This research was also supported by the Pioneer Research Center Program through the National Research Foundation of Korea funded by the Ministry of Science, ICT & Future Planning (grant No.2022M3C1A3081211).

Conflict of Interest

The authors declare no conflict of interest.

Data Availability Statement

The data that support the findings of this study are available from the corresponding author upon reasonable request.

Keywords

Ag nanowires, cold pressing, interfacial adhesions, segmental motion, solvated polymer chains

Received: September 26, 2022

Revised: November 24, 2022

Published online:

- [1] Y. Lee, J. W. Chung, G. H. Lee, H. Kang, J.-Y. Kim, C. Bae, H. Yoo, S. Jeong, H. Cho, S.-G. Kang, J. Y. Jung, D.-W. Lee, S. Gam, S. G. Hahm, Y. Kuzumoto, S. J. Kim, Z. Bao, Y. Hong, Y. Yun, S. Kim, *Sci. Adv.* **2021**, *7*, eabg9180.
- [2] N. Matsuhisa, S. Niu, S. J. K. O'Neill, J. Kang, Y. Ochiai, T. Katsumata, H.-C. Wu, M. Ashizawa, G.-J. N. Wang, D. Zhong, X. Wang, X. Gong, R. Ning, H. Gong, I. You, Y. Zheng, Z. Zhang, J. B. H. Tok, X. Chen, Z. Bao, *Nature* **2021**, *600*, 246.
- [3] N. Liu, A. Chortos, T. Lei, L. Jin, T. R. Kim, W.-G. Bae, C. Zhu, S. Wang, R. Pfattner, X. Chen, R. Sinclair, Z. Bao, *Sci. Adv.* **2017**, *3*, e1700159.
- [4] J. Xu, S. Wang, G.-J. N. Wang, C. Zhu, S. Luo, L. Jin, X. Gu, S. Chen, V. R. Feig, J. W. F. To, S. Rondeau-Gagné, J. Park, B. C. Schroeder, C. Lu, J. Y. Oh, Y. Wang, Y.-H. Kim, H. Yan, R. Sinclair, D. Zhou, G. Xue, B. Murmann, C. Linder, W. Cai, J. B.-H. Tok, J. W. Chung, Z. Bao, *Science* **2017**, *355*, 59.
- [5] S. Lee, D. Sasaki, D. Kim, M. Mori, T. Yokota, H. Lee, S. Park, K. Fukuda, M. Sekino, K. Matsuura, T. Shimizu, T. Someya, *Nat. Nanotechnol.* **2019**, *14*, 156.
- [6] C. Wang, D. Hwang, Z. Yu, K. Takei, J. Park, T. Chen, B. Ma, A. Javey, *Nat. Mater.* **2013**, *12*, 899.
- [7] H. Zhou, T.-W. Lee, *IEEE Spectrum* **2020**, *57*, 24.
- [8] H. Zhou, J. Park, Y. Lee, J.-M. Park, J.-H. Kim, J. S. Kim, H. D. Lee, X. Cai, L. Li, X. Sheng, H. J. Yun, J.-W. Park, J.-Y. Sun, T.-W. Lee, *Adv. Mater.* **2020**, *32*, 2001989.
- [9] Y. Lee, H. Zhou, T.-W. Lee, *J. Mater. Chem. C* **2018**, *6*, 3538.
- [10] H. Zhou, S. J. Han, H.-D. Lee, D. Zhang, M. Anayee, S. H. Jo, Y. Gogotsi, T.-W. Lee, *Adv. Mater.* **2022**, 2206377.
- [11] D. Yin, N.-R. Jiang, Z.-Y. Chen, Y.-F. Liu, Y.-G. Bi, X.-L. Zhang, J. Feng, H.-B. Sun, *Adv. Opt. Mater.* **2020**, *8*, 1901525.
- [12] M. S. Lim, M. Nam, S. Choi, Y. Jeon, Y. H. Son, S.-M. Lee, K. C. Choi, *Nano Lett.* **2020**, *20*, 1526.
- [13] D. K. Choi, D. H. Kim, C. M. Lee, H. Hafeez, S. Sarker, J. S. Yang, H. J. Chae, G.-W. Jeong, D. H. Choi, T. W. Kim, S. Yoo, J. Song, B. S. Ma, T.-S. Kim, C. H. Kim, H. J. Lee, J. W. Lee, D. Kim, T.-S. Bae, S. M. Yu, Y.-C. Kang, J. Park, K.-H. Kim, M. Sujak, M. Song, C.-S. Kim, S. Y. Ryu, *Nat. Commun.* **2021**, *12*, 2864.
- [14] D. Yin, J. Feng, R. Ma, Y.-F. Liu, Y.-L. Zhang, X.-L. Zhang, Y.-G. Bi, Q.-D. Chen, H.-B. Sun, *Nat. Commun.* **2016**, *7*, 11573.
- [15] T. Yokota, P. Zalar, M. Kaltenbrunner, H. Jinno, N. Matsuhisa, H. Kitanosako, Y. Tachibana, W. Yukita, M. Koizumi, T. Someya, *Sci. Adv.* **2016**, *2*, e1501856.
- [16] C. Larson, B. Peele, S. Li, S. Robinson, M. Totaro, L. Beccai, B. Mazzolai, R. Shepherd, *Science* **2016**, *351*, 1071.
- [17] X. Shi, Y. Zuo, P. Zhai, J. Shen, Y. Yang, Z. Gao, M. Liao, J. Wu, J. Wang, X. Xu, Q. Tong, B. Zhang, B. Wang, X. Sun, L. Zhang, Q. Pei, D. Jin, P. Chen, H. Peng, *Nature* **2021**, *591*, 240.
- [18] Y. J. Tan, H. Godaba, G. Chen, S. T. M. Tan, G. Wan, G. Li, P. M. Lee, Y. Cai, S. Li, R. F. Shepherd, J. S. Ho, B. C. K. Tee, *Nat. Mater.* **2020**, *19*, 182.
- [19] D. Son, J. Kang, O. Vardoulis, Y. Kim, N. Matsuhisa, J. Y. Oh, J. W. To, J. Mun, T. Katsumata, Y. Liu, A. F. McGuire, M. Krason, F. Molina-Lopez, J. Ham, U. Kraft, Y. Lee, Y. Yun, J. B. Tok, Z. Bao, *Nat. Nanotechnol.* **2018**, *13*, 1057.
- [20] J.-M. Park, J. Park, Y.-H. Kim, H. Zhou, Y. Lee, S. H. Jo, J. Ma, T.-W. Lee, J.-Y. Sun, *Nat. Commun.* **2020**, *11*, 4638.
- [21] M. S. White, M. Kaltenbrunner, E. D. Glowacki, K. Gutnichenko, G. Kettlgruber, I. Graz, S. Aazou, C. Ulbricht, D. A. M. Egbe, M. C. Miron, Z. Major, M. C. Scharber, T. Sekitani, T. Someya, S. Bauer, N. S. Sariciftci, *Nat. Photonics* **2013**, *7*, 811.
- [22] J. Liang, L. Li, X. Niu, Z. Yu, Q. Pei, *Nat. Photonics* **2013**, *7*, 817.
- [23] Y. Zhibin, N. Xiaofan, L. Zhitian, P. Qibing, *Adv. Mater.* **2011**, *23*, 3989.
- [24] J. Liu, J. Wang, Z. Zhang, F. Molina-Lopez, G.-J. N. Wang, B. C. Schroeder, X. Yan, Y. Zeng, O. Zhao, H. Tran, T. Lei, Y. Lu, Y.-X. Wang, J. B. H. Tok, R. Dauskardt, J. W. Chung, Y. Yun, Z. Bao, *Nat. Commun.* **2020**, *11*, 3362.
- [25] J. Liang, L. Li, K. Tong, Z. Ren, W. Hu, X. Niu, Y. Chen, Q. Pei, *ACS Nano* **2014**, *8*, 1590.
- [26] J. H. Kim, J. W. Park, *Sci. Adv.* **2021**, *7*, eabd9715.
- [27] Z. Zhang, W. Wang, Y. Jiang, Y.-X. Wang, Y. Wu, J.-C. Lai, S. Niu, C. Xu, C.-C. Shih, C. Wang, H. Yan, L. Galuska, N. Prine, H.-C. Wu, D. Zhong, G. Chen, N. Matsuhisa, Y. Zheng, Z. Yu, Y. Wang, R. Dauskardt, X. Gu, J. B. H. Tok, Z. Bao, *Nature* **2022**, *603*, 624.
- [28] H. Zhou, S. J. Han, A. K. Harit, D. H. Kim, D. Y. Kim, Y. S. Choi, H. Kwon, K. N. Kim, G. T. Go, H. J. Yun, B. H. Hong, M. C. Suh, S. Y. Ryu, H. Y. Woo, T.-W. Lee, *Adv. Mater.* **2022**, *34*, 2203040.
- [29] Y. Liu, M. Zhu, J. Sun, W. Shi, Z. Zhao, X. Wei, X. Huang, Y. Guo, Y. Liu, *Adv. Mater.* **2022**, *34*, 2201844.
- [30] H. Zhou, J.-W. Park, *Org. Electron.* **2015**, *24*, 272.
- [31] H. Zhou, J.-W. Park, *Thin Solid Films* **2016**, *619*, 281.
- [32] Y. Liu, J. Zhang, H. Gao, Y. Wang, Q. Liu, S. Huang, C. F. Guo, Z. Ren, *Nano Lett.* **2017**, *17*, 1090.
- [33] F. M. Cabrerizo, J. Arnbjerg, M. P. Denofrio, R. Erra-Balsells, P. R. Ogilby, *ChemPhysChem* **2010**, *11*, 796.
- [34] J. Y. Oh, Z. Bao, *Adv. Sci.* **2019**, *6*, 1900186.
- [35] T. Lei, J.-H. Dou, X.-Y. Cao, J.-Y. Wang, J. Pei, *J. Am. Chem. Soc.* **2013**, *135*, 12168.
- [36] T. M. Brown, R. H. Friend, I. S. Millard, D. J. Lacey, J. H. Burroughes, F. Cacialli, *Appl. Phys. Lett.* **2000**, *77*, 3096.
- [37] H. Gao, S. Chen, J. Liang, Q. Pei, *ACS Appl. Mater. Interfaces* **2016**, *8*, 32504.
- [38] E. J. Sawyer, A. V. Zaretski, A. D. Printz, N. V. de los Santos, A. Bautista-Gutierrez, D. J. Lipomi, *Extreme Mech Lett* **2016**, *8*, 78.